

# On acoustically modulated jet shear layers and the Nyquist–Shannon sampling theorem

Cite as: Phys. Fluids **34**, 115106 (2022); <https://doi.org/10.1063/5.0118025>

Submitted: 03 August 2022 • Accepted: 02 October 2022 • Accepted Manuscript Online: 04 October 2022 • Published Online: 02 November 2022

Published open access through an agreement with JISC Collections

 C. J. Nicholls,  K. Chakravarthy,  B. M. T. Tang, et al.



View Online



Export Citation



CrossMark

## ARTICLES YOU MAY BE INTERESTED IN

[Flame acceleration and transition to detonation in a pre-/main-chamber combustion system](#)

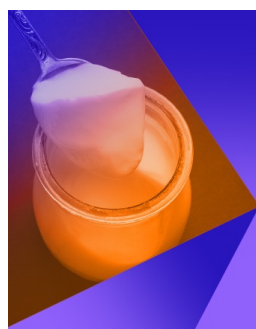
Physics of Fluids **34**, 116105 (2022); <https://doi.org/10.1063/5.0122240>

[Influence of non-uniform thermal boundary on flow and heat transfer characteristics in rectangular channel](#)

Physics of Fluids **34**, 115105 (2022); <https://doi.org/10.1063/5.0118139>

[Airfoil trailing-edge noise and drag reduction at a moderate Reynolds number using wavy geometries](#)

Physics of Fluids **34**, 117107 (2022); <https://doi.org/10.1063/5.0120124>



## Physics of Fluids

## Special Topic: Food Physics

**Submit Today!**

# On acoustically modulated jet shear layers and the Nyquist–Shannon sampling theorem

Cite as: Phys. Fluids **34**, 115106 (2022); doi: [10.1063/5.0118025](https://doi.org/10.1063/5.0118025)

Submitted: 3 August 2022 · Accepted: 2 October 2022 ·

Published Online: 2 November 2022



View Online



Export Citation



CrossMark

C. J. Nicholls,<sup>a)</sup> K. Chakravarthy, B. M. T. Tang, B. A. O. Williams, and M. Bacic

## AFFILIATIONS

Department of Engineering Science, University of Oxford, Oxford OX2 0ES, United Kingdom

<sup>a)</sup> Author to whom correspondence should be addressed: [christopher.nicholls@eng.ox.ac.uk](mailto:christopher.nicholls@eng.ox.ac.uk)

## ABSTRACT

The goal of this paper is to present the behavior of a jet shear layer in response to acoustic excitation from a signal processing perspective. The main idea is that the vortices that roll-up in the jet shear layer are similar to the discrete samples of a digital control system, and, hence, that the Nyquist–Shannon sampling theorem should apply. We further hypothesize that the strength of a vortex is determined by the mean amplitude of the excitation waveform during its creation. We also argue that, at least in some cases, demodulation occurs as a result of the vorticity signal generated by the convection of discrete vortices past a point in the shear layer. This vorticity signal is related to the amplitude modulation (AM) excitation waveform by a half-wave rectification operation, a common implementation of an AM demodulator. To investigate these ideas, a free, round jet that is excited upstream of the nozzle is studied using particle image velocimetry. Experiments are conducted that confirm that the sampling theorem applies, and an aliased response is observed when the Nyquist limit is exceeded. Previous authors have attributed demodulation to a vortex merging mechanism, but we demonstrate that merging is not always required for demodulation and suggest that it is one of two mechanisms at play.

© 2022 Author(s). All article content, except where otherwise noted, is licensed under a Creative Commons Attribution (CC BY) license (<http://creativecommons.org/licenses/by/4.0/>). <https://doi.org/10.1063/5.0118025>

## I. INTRODUCTION

This paper presents a signal processing perspective on the response of shear layers to modulated perturbations. When a sinusoidal perturbation with sufficient amplitude excites a shear layer, vortices roll up and are shed at the frequency of the perturbation.<sup>1</sup> For a fixed perturbation frequency, the perturbation amplitude determines the degree of the variation in vorticity and hence mixing and entrainment—these quantities constitute the shear layer response. Modulating the amplitude of the perturbation results in the shear layer responding at the modulating signal frequency. This property was discovered by Wiltse and Glezer<sup>2</sup> and is called shear layer demodulation. Modulated perturbations have been widely used in flow control applications to exploit this property. Examples in the literature include jet thrust vectoring,<sup>3,4</sup> piezo-fluidic amplifier control,<sup>5</sup> and boundary layer control.<sup>6</sup> The demodulation effect has also been observed in synthetic jet actuators, as demonstrated by Yehoshua and Seifert.<sup>7</sup>

Vukasinovic *et al.*<sup>8</sup> investigated the mechanism within the shear layer that causes the demodulation. They studied the flow over a backward-facing step controlled by a wall-normal synthetic jet actuator mounted upstream of the step. The synthetic jet was driven with a carrier frequency of  $f_c = 2000$  Hz, with a square wave modulating

signal with frequencies in the range  $f_m = 50$ – $300$  Hz. Phase-locked particle image velocimetry (PIV) vorticity snapshots at several times through a modulation period at  $f_m = 100$  Hz show the vortex train being produced at the carrier tone frequency,  $f_c = 2000$  Hz, during the positive portion of the period only (opposite-sense vortices are produced on the ingestion stroke of the actuator, but these are dissipated rapidly). The snapshots indicate that the vortices produced during the “on” portion of the modulating period coalesce into a larger vortex at the modulating frequency. The phase-locked velocity profiles provided at several downstream distances demonstrate that the excitation varies the degree of separation over the step at the modulating frequency, resulting from the variation in entrainment.

Yehoshua and Seifert<sup>7</sup> explained the mechanisms by which synthetic jet actuators demodulate amplitude modulation (AM) excitation signals. A zero-net mass flux (ZNMF) actuator was used in otherwise still air to produce a train of vortex pairs at the carrier frequency,  $f_c$ , whose strength and speed were determined by the amplitude of the modulating signal at the time of their production. Vortex pairs that had insufficient speed to escape the ingestion stroke of the actuator were denoted sub-critical. These were vortices produced when the modulating signal was below a critical amplitude threshold. For the

supercritical vortices, merging and leap-frogging events led to the largest vortex pairs absorbing others. As such, some distance away from the actuator, only one vortex pair per modulating tone period persisted.

In their initial discovery of the demodulation property of shear layers, Wiltse and Glezer<sup>2</sup> conducted an experiment to determine the working mechanism. The flow speed was reduced to 2.75 m/s (although it was only 4 m/s for the rest of the experiments), and Schlieren photographs were provided, showing the flow at several phases in the modulating period. Wiltse and Glezer<sup>2</sup> highlight line vortices produced in the shear layer at the carrier tone frequency ( $f_c = 510$  Hz), which roll up into larger vortices at the modulating frequency ( $f_m = 12$  Hz) further downstream.

The vortex-interaction demodulation mechanism described in these studies has two key features: vortices are produced at the carrier frequency,  $f_c$ , and there is a requirement for many vortices to merge into a single vortex at the modulating frequency. In the case of Wiltse and Glezer,<sup>2</sup>  $f_c/f_m = 510/12 = 42.5$  vortices are required on average to be present in the shear layer simultaneously to produce a single vortex at the modulating frequency. The number of vortices present can be estimated by the ratio of the average distance between vortices and the streamwise length, in which the vortices exist before they break down into isotropic turbulence.

Results from PIV experiments conducted by Mair<sup>9</sup> indicate a vortex convection speed of around 65% of the centerline jet velocity. Similarly, Kuo *et al.*<sup>10</sup> reported a vortex convection speed of 67% of the jet centerline velocity. If the convection speed is assumed to be  $v_{SL} \approx 0.65U$ , where  $U$  is the mean velocity, the range of values for the distance between vortices in Wiltse and Glezer<sup>2</sup> is given by

$$L_v = v_{SL}/f_c \approx 3.5 \text{ mm} = 0.082 D_h, \quad (1)$$

where  $D_h = 43.0$  mm is the hydraulic diameter of the square jet,  $L_v$  is the distance between vortices, and  $v_{SL}$  is the vortex convection speed. A first approximation for the length along which vortices exist is the length of the potential core, although they do persist beyond this region for some distance before breaking down into isotropic turbulence. Mair *et al.*<sup>11</sup> reported potential core lengths ranging from  $3D$  when excited at the jet preferred mode to  $7D$  when unexcited. To get a sense of the order of the average number of vortices present in the shear layer, the length of the region where vortices at  $f_c$  exist is taken to be  $L_{ve} \approx 5D_h$ . This gives the number of vortices present at the carrier frequency as

$$N_v = \frac{L_{ve}}{L_v} \approx 61, \quad (2)$$

so that on average there should be  $61/42.5 = 1.4$  vortices present at the modulating frequency ( $f_m = 12$  Hz). The merging mechanism proposed by Wiltse and Glezer,<sup>2</sup> therefore, seems plausible. However, the flow speed in question was very low, so that there were many vortices present simultaneously at  $f_c$  to roll up into vortices at  $f_m$ . This mechanism does not explain how demodulation can occur when this is not the case, for example, if  $f_m$  were reduced to 1 Hz for the same  $f_c$  and flow conditions.

The characteristic frequency of a shear layer, or shear layer mode, is defined as the frequency at which an unexcited shear layer rolls up and sheds vortices.<sup>12</sup> It depends on the initial momentum thickness,

i.e., the boundary layer thickness at the nozzle orifice in the case of a jet, and is determined by the following relationship:

$$St_\theta = \frac{f_n \theta}{u_0} \approx 0.012, \quad (3)$$

where  $f_n$  is the most amplified frequency,  $\theta$  is the momentum thickness at the nozzle orifice, and  $u_0$  is the jet centerline velocity.<sup>12</sup> A second, relevant characteristic frequency is the jet preferred mode, first studied by Crow and Champagne,<sup>1</sup> which refers to the frequency of excitation that maximizes the entrainment rate and, hence, the rate of jet spreading. For a round jet, the preferred mode is defined by

$$St_D = \frac{f_{ex} D}{u_0} \approx 0.3, \quad (4)$$

where  $f_{ex}$  is the excitation frequency and  $D$  is the jet diameter.<sup>1</sup> The relationship between these two modes is an active area of research with numerous studies published in recent years.<sup>10,13</sup> When exciting the jet preferred mode, the excitation amplitude required to produce vortex shedding that is locked onto the excitation frequency is at a minimum. However, lock-on can be induced away from the preferred (or any other) mode if the excitation amplitude is large enough.<sup>11</sup>

In this paper, a free, round jet is excited upstream of the nozzle orifice with a loudspeaker and studied with particle image velocimetry (PIV). It is shown that the lock-on effect occurs, and the vortices are produced at the excitation frequency in most cases. We argue that the accepted mechanism for shear layer demodulation, that vortex merging events are the cause, requires amendment. It is demonstrated that modulating the excitation waveform modulates the strength of the vortices produced, but that these vortices do not necessarily merge. Taking the signal processing perspective further leads to the notion that the vortices “sample” the modulating signal at the carrier tone frequency to determine their strength. Discrete vortices are, therefore, akin to samples in a digital system. The vorticity signal measured at a point in the shear layer is shown to resemble a half-wave rectified version of the AM excitation waveform. Since a half-wave rectifier is a common implementation of an AM demodulator, this explains a mechanism by which the excitation waveform can be demodulated by the shear layer that does not require vortex merging. The corollary of the “sampling” model is that the Nyquist–Shannon sampling theorem should apply, and modulating signal frequencies exceeding half the carrier frequency, i.e.,  $f_m > f_c/2$ , should result in an aliased response at  $f_c - f_m$  instead of at  $f_m$ .<sup>14,15</sup>

We present the signal processing perspective of the shear layer response to excitation in Sec. III after the experimental setup is described in Sec. II. The results are given in Sec. IV and discussed in Sec. V, after which conclusions are drawn in Sec. VI.

## II. EXPERIMENTAL METHODS

The test section is shown in Fig. 1. An air jet emerges from a nozzle into an acrylic box with two outlets on the opposite face. These outlets are joined by flexible hose and connected to a building exhaust system, which provides a small back pressure to the flow. The nozzle has a 7.5 mm diameter circular cross-section and is 165 mm long. The hole in the box through which the nozzle supplies the flow was drilled off-perpendicular to the plate, such that the jet is not perfectly straight. The extent of its angle is apparent in the baseline data presented in Sec. IV. The flow is excited by a loudspeaker upstream of the nozzle in

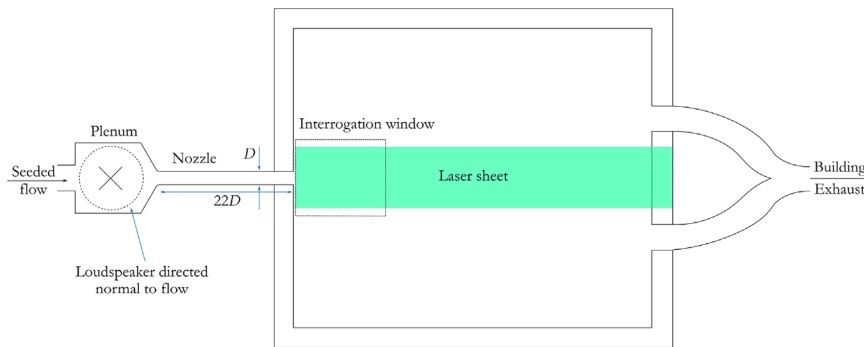


FIG. 1. Free jet test section setup.

a plenum, with the loudspeaker (the 10 W Visaton FR 58) directed perpendicularly to the streamwise direction. The loudspeaker is driven by a 40 W power amplifier (Kemo Electronic M034N), which is connected to a signal generator. The flow is seeded with di-ethyl-hexyl-sebacate (DEHS) using a LaVision aerosol generator. The drop-let size ranges between 0.1 and 1  $\mu\text{m}$ . The particle density and flow rate are controlled by two mass flow controllers (both Omega FMA-2612A) and a bypass route, both upstream of the test section and supplied by a lab ring-main air supply. The mass flow controllers have a combined error of  $\pm 2.8\%$  in the mass flow rate. The light sheet from a dual-head Nd:YAG New Wave Gemini PIV 200–15 laser that produces a beam at 532 nm with 14 mJ per pulse is used to reproduce the velocity vector field of the jet from the nozzle orifice to around eight nozzle widths downstream. The laser is passed through a cylindrical and spherical lenses of focal length 90 and 350 mm, respectively, to form it into a sheet less than 0.5 mm thick and 2.5 nozzle widths wide. Image pairs are acquired using a charge-coupled device (CCD) camera (Bobcat B1621M) with a fixed inter-frame time of 200 ns. A calibration grid is used to set the focus, correct for optical distortion, and scale the vector units to m/s.

The laser inter-pulse time is set to 10.5  $\mu\text{s}$ . A standard, decreasing window size, multipass processing scheme is used to calculate the velocity vector field. The three passes use  $128 \times 128$ ,  $64 \times 64$ , and  $32 \times 32$  pixel interrogation window sizes. Spatial resolution is improved through use of an overlap of 50% for all passes. The resulting discretization of the flow field is a grid with a spacing of 0.08 nozzle widths between stations. A vector-validation filter is used that removes anomalous vectors that exceed a predetermined range and interpolates the surrounding vector field to replace them. The Stokes number based on the maximum particle size, the nozzle diameter, and the average nozzle velocity is below 0.01. Errors associated with tracing accuracy are, therefore, bounded to be less than 1%. The laser and camera are triggered at or close to 10 Hz. When exactly 10 Hz, events occurring at multiples of 10 Hz are aliased onto DC. It is important to distinguish between the aliasing that occurs as a result of the low sampling frequency (phase-averaging) and the aliasing in the shear layer that is the subject of this paper. The trigger generator does not time the signal generator, and, consequently, the input waveform phase is not known relative to the phase of the measurements. Scatter from the nozzle corrupts the measurements in a narrow region immediately downstream of the nozzle approximately  $0.1 D$  long. The flow rate used was 1.06 g/s for all free jet experiments. This corresponds to a Reynolds number based on jet diameter of approximately  $10^4$ .

### III. SIGNAL PROCESSING PERSPECTIVE

The main idea of this paper is that the vortices that roll-up in the jet shear layer are similar to the discrete samples of a digital control system. We hypothesize that the strength of a vortex is determined by the mean amplitude of the excitation waveform during its creation, which was observed by Yehoshua and Seifert<sup>7</sup> for the case of a synthetic jet in still air. This is represented graphically in Fig. 2, which shows the carrier waveform, the signal that modulates its amplitude, the resulting AM signal that is used to excite the jet, the vortex train in the shear layer in response, and the vorticity of that vortex train that would be measured by a point in the shear layer. The size of each vortex in the figure was determined by taking the average value of the modulating signal during the negative half period in each carrier waveform, and represents the vortex strength. This choice was arbitrary—sampling any fraction of the carrier period would work. The opposite-sense vortices that could, in theory, be created during the positive half of the carrier period are assumed not to be occur because of the natural offset of the shear layer vorticity. Opposite-sense vortices were not observed in any of the experiments, which supports this approach. The vorticity signal observed by a point in the shear layer is modeled as the half-wave rectified AM excitation signal. This captures the essence of how vortices redistribute vorticity in the shear layer, which is demonstrated by a comparison of the vortex train and the vorticity signal in Fig. 2. To clarify, Figs. 2 and 3 are hypothetical, illustrative diagrams rather than data.

With a constant-amplitude excitation tone, the vortex size is constant. In the case of 100% AM, the waveform is given by

$$g(t) = \sin(2\pi f_c t) (A + A \sin(2\pi f_m t)), \quad (5)$$

and the vortex size resembles a sampled version of the envelope of the AM signal. The effect of this modulated vortex size is a modulation of the shear layer vorticity, which is consistent with the vorticity signal in Fig. 2.

As the modulation frequency,  $f_m$ , increases, the number of carrier tone periods (or “samples”) per period of the modulating tone decreases. When  $f_m = f_c/2$ , there will be only two different sizes of vortex produced in the shear layer. If  $f_m$  is increased beyond  $f_c/2$ , the shear layer response decreases below  $f_c/2$ . The cases for  $f_m = f_c/2$  (the Nyquist limit) and  $f_m = 0.75f_c$  are shown in Fig. 3. In the case where  $f_m = 0.75f_c$  in Fig. 3(b), the shear layer response frequency is clearly lower than the Nyquist limit case in Fig. 3(a). The Nyquist–Shannon sampling theorem indicates that the response is aliased to  $f_c - f_m = 0.25f_c$ . The diagram for the case  $f_m = 0.25f_c$  is

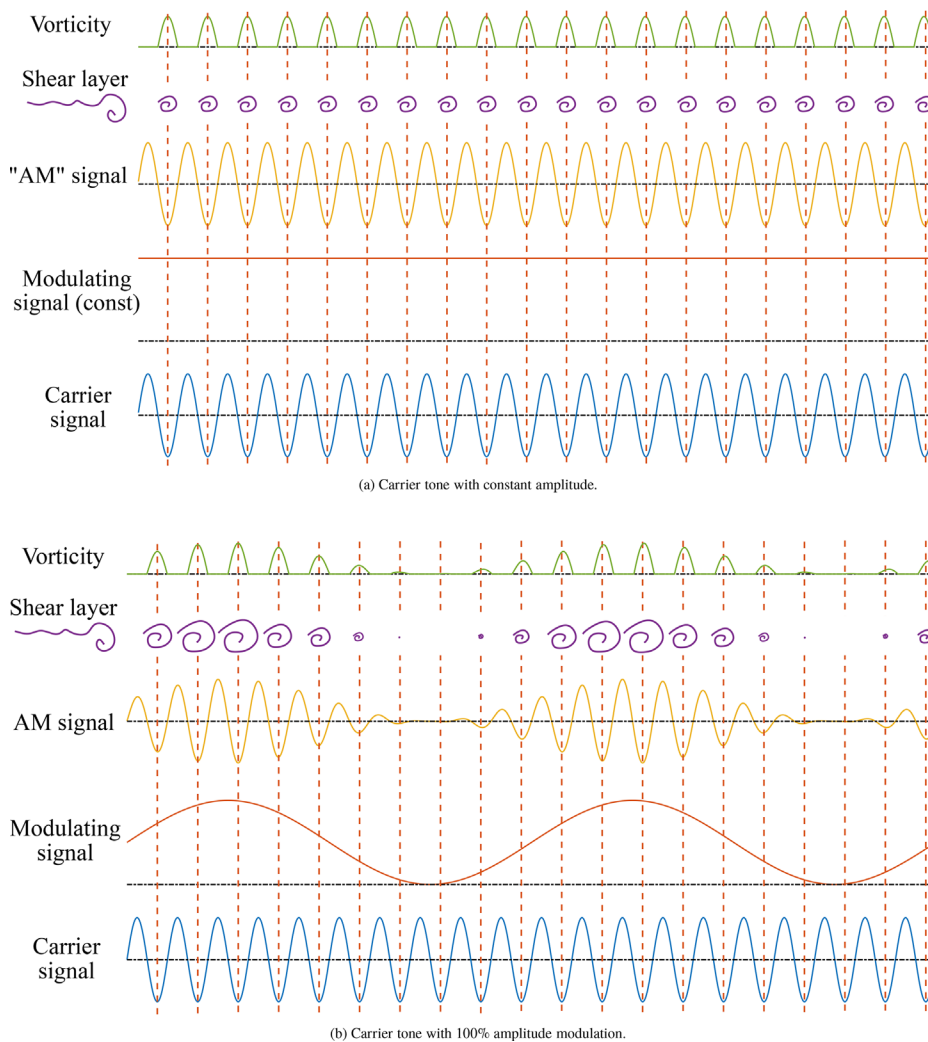


**FIG. 2.** Shear layer response to constant carrier tone (constant modulation “signal”) (a) and 100% amplitude modulation signal (b);  $u_{SL}(t)$ : constant, 100% AM. (a) Carrier tone with constant amplitude. (b) Carrier tone with 100% amplitude modulation.

shown in Fig. 3(c) for comparison. The shear layer response and vorticity signal are phase-shifted versions of those in Fig. 3(b), but the envelope is otherwise the same.

The demodulation occurs because the vorticity signal caused by the vortex train is a rectified signal. A half-wave rectifier is a common implementation of an AM demodulator. The envelope of the vorticity signal is, therefore, present at baseband, although it also remains partially modulated onto the carrier because half-wave rectification is an incomplete demodulation.

#### IV. RESULTS

The unexcited free jet with a flow rate of 1.06 g/s was sampled for 250 PIV frames at 10 Hz. The time-mean velocity profile at a station 0.16 nozzle widths downstream of the nozzle orifice is shown in Fig. 4. The average value across a single nozzle width at the center of the profile is of  $U = 20.3 \pm 0.2$  m/s. This implies a density of  $1.19 \pm 0.05$  kg/m<sup>3</sup>. An example of a single, raw image is shown in Fig. 5. The time-averaged, processed flow field is shown in Fig. 6, where the color represents velocity magnitude. This figure illustrates the non-perpendicular

orientation of the jet described in Sec. II. The jet does not come close to the sides of the box, so the angle has a negligible effect on the results. The vorticity of the time-averaged flow field from the same experiment is shown in Fig. 7. For comparison, the vorticity of a single, instantaneous flow field snapshot from the experiment is shown in Fig. 8. The coherent structures present in a single flow field are removed by the averaging. This is because the natural vortex shedding frequency is not a multiple of the triggering frequency so is aliased onto a frequency other than DC.

The frequency corresponding to the jet preferred mode can be calculated using (4), and the jet centerline velocity value from Fig. 4 to be  $f \approx 920$  Hz. The momentum thickness was computed numerically using each side of the velocity profile in Fig. 4 to give a mean and difference of  $\theta = 0.0340 \pm 0.0028 D$ . This value is consistent with the calculations of Mair *et al.*<sup>11</sup> who used a nearly identical test section and experimental setup. The frequency corresponding to the shear layer mode can then be calculated from (3) to be  $f_n = 1080 \pm 89$  Hz.

Figure 9 plots the vorticity of the ensemble-averaged flow field ( $N = 100$  PIV frames), where the upstream loudspeaker was exciting



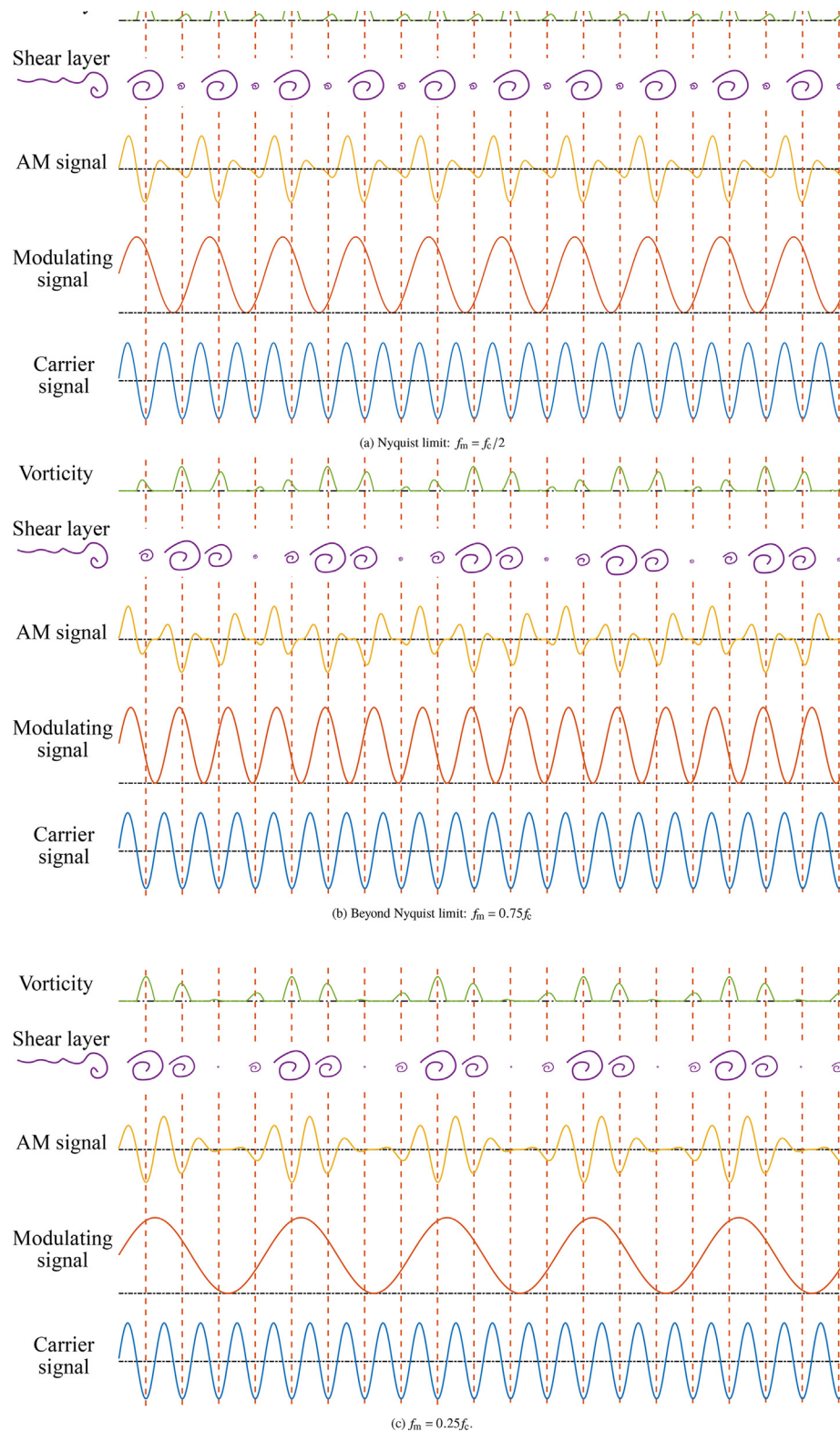


FIG. 3. Shear layer response to 100% AM tones at Nyquist limit and beyond. (a) Nyquist limit:  $f_m = f_c/2$ . (b) Beyond Nyquist limit:  $f_m = 0.75f_c$ . (c)  $f_m = 0.25f_c$ .

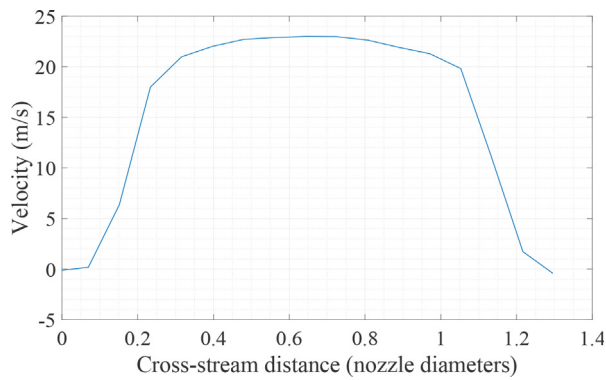


FIG. 4. Unexcited, time-mean velocity profile  $0.16D$  downstream of the nozzle orifice.

the flow with a constant amplitude tone at 1 kHz. The flow field shows a 2D slice through two vortex rings that are produced as a result of the excitation. This appears as two pairs of vortices in the same physical location in each snapshot because, unlike in the unexcited case, they are created at a harmonic of the triggering frequency, and so the vortex generation process is aliased onto DC. Repeating the experiment with a set of random start times leads to an ensemble of such flow fields showing the progress of the vortices at different phases. This demonstrates that the vortex shedding frequency has locked onto the excitation frequency or some derivative of it. This is expected due to the proximity of the excitation frequency to both the shear layer mode and jet preferred mode frequencies. In order to judge whether the vortices are shed at the excitation frequency rather than a (sub-)harmonic, a line was drawn through each side of the shear layer, like the one shown in Fig. 9, and the vorticity and velocity magnitude were plotted along it. For this example, the vorticity and velocity magnitude along

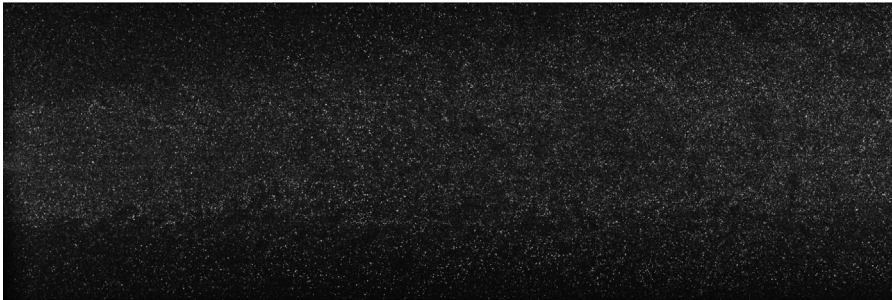


FIG. 5. Example raw image of unexcited free jet.

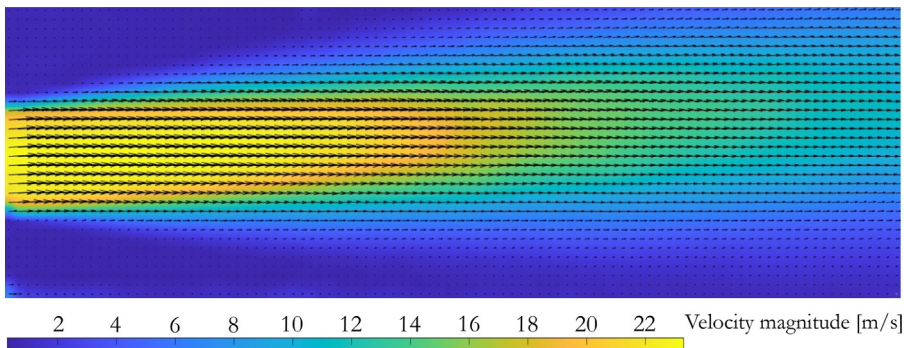


FIG. 6. Velocity magnitude of time-averaged, unexcited free jet.

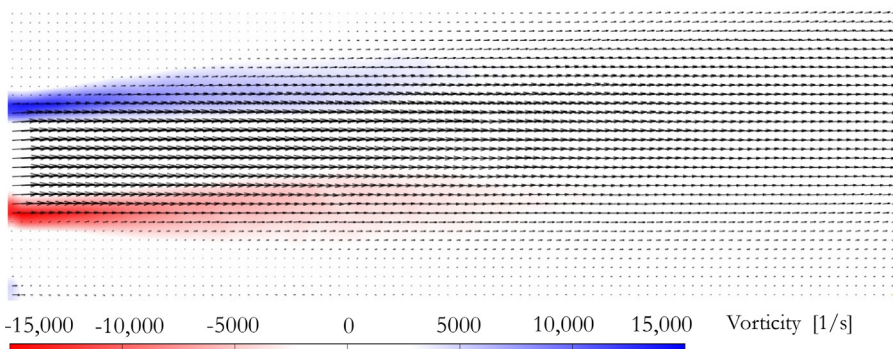


FIG. 7. Vorticity of time-averaged, unexcited free jet.

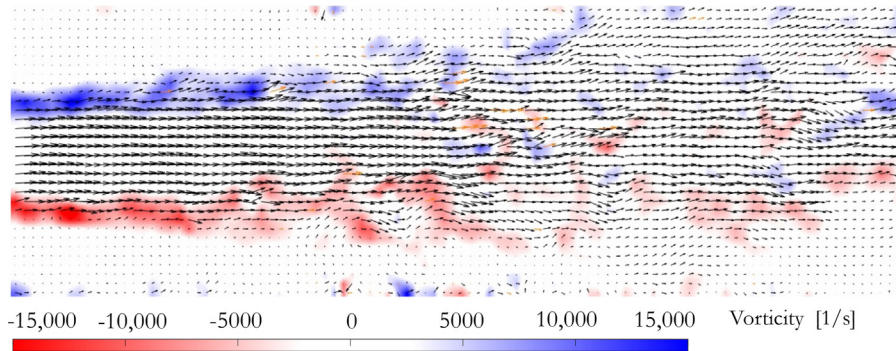


FIG. 8. Vorticity of single snapshot of unexcited free jet.

the line are shown in Fig. 10. The local maximum in vorticity around each vortex was used to identify the centers, and the average of the velocity magnitudes at those points ( $v_1$  and  $v_2$  in Fig. 10) was used to give an indication of convection speed,  $v_{SL}$ . The vortex shedding frequency can then be determined by the ratio of the convection speed to the vortex spacing. The vortex spacing given by this method ( $x_2 - x_1$  in Fig. 10) is relatively insensitive to the line chosen, but this is not true of the convection speed estimate. However, since our purpose is solely to judge if the vortices are produced at the excitation frequency or a (sub-)harmonic, the method is sufficient.

A similar line was used on the other side of the jet, and the average of the vortex spacing and temporal frequency on both sides was calculated. This was repeated for a range of other excitation frequencies using the same line. Since vortices are expected to convect at the same speed, the ensemble of estimated convection speeds was used to produce values for the mean and standard deviation of the convection speed, given by

$$\mu_{v,SL} = 12.7 \text{ m/s} = 0.63 U; \quad \sigma_{v,SL} = 0.99 \text{ m/s} = 0.049 U, \quad (6)$$

where  $U$  is the mean jet velocity. The value of  $\mu_{v,SL}$  is in agreement with the values reported in the literature, which are  $0.65 U^9$  and  $0.67 U^{10}$ . The mean value was used along with the estimated vortex spacing to compute a mean shedding frequency in each case. The standard deviation in the convection speed was combined with an assumed  $0.1 D$  uncertainty in the vortex spacing estimate to produce

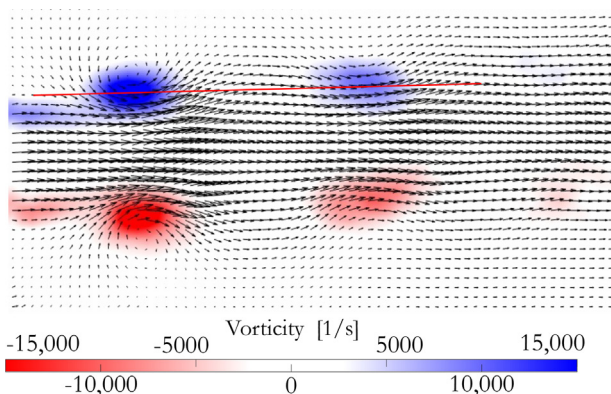


FIG. 9. Vorticity of time-averaged free jet with 1 kHz excitation, with line used for estimating vortex spacing and shedding frequency in the upper shear layer.

bounds on the shedding frequency. The resulting vortex spacing and temporal frequency are plotted against excitation frequency in Fig. 11. Also shown plotted are the calculated bounds for the shear layer mode frequency and the jet preferred mode frequency, which were computed using (3) and (4), respectively. The value of the vortex shedding frequency equal to (locked on to) the excitation frequency is plotted, along with the bounds on the curve of the expected vortex spacing for the same condition. The expected vortex spacing was calculated from

$$L_{v,exp} = \frac{v_{SL}}{f_{ex}}, \quad (7)$$

where  $v_{SL}$  is the estimated vortex convection speed and  $f_{ex}$  is the excitation frequency. It was not possible to determine the convection speed for the  $f_{ex} = 300 \text{ Hz}$  case because there was only ever one vortex present in the shear layer. To estimate the shedding frequency in this case, the periodicity of the flow field was found by reducing the laser triggering frequency fractionally from  $10 \text{ Hz}$ , such that any event occurring at  $300 \text{ Hz}$  was aliased to a very low frequency. A full picture

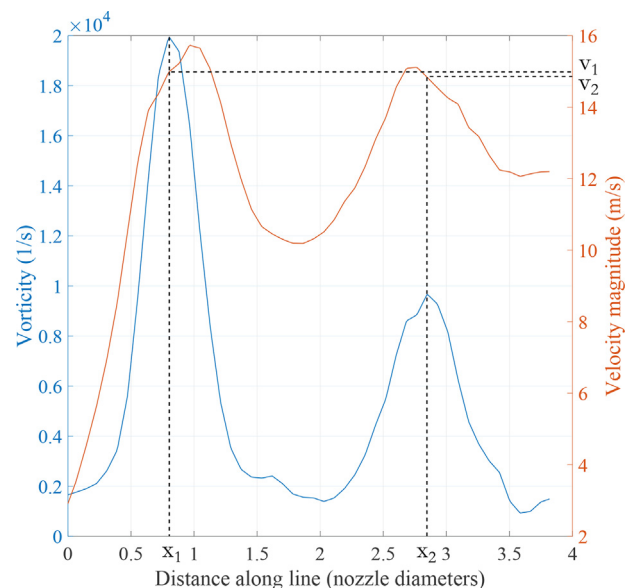
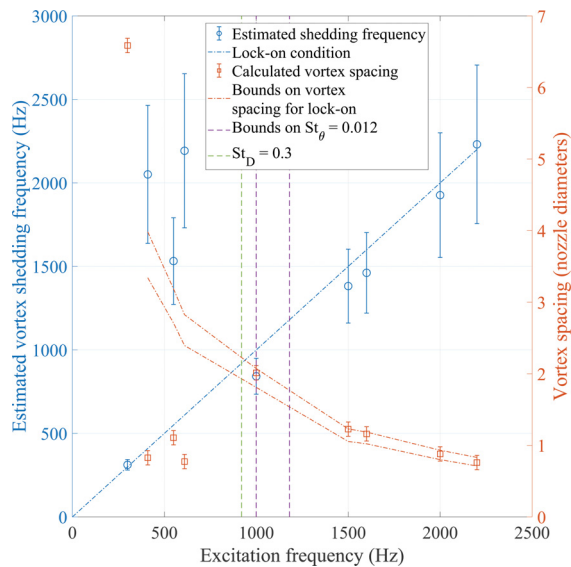


FIG. 10. Vorticity and velocity magnitude along line (downstream direction) in upper shear layer of time-averaged free jet with 1 kHz excitation.





**FIG. 11.** Estimated vortex shedding frequency (blue circles), vortex shedding frequency for lock-on to excitation frequency (dash-dot blue), estimated vortex spacing (red squares), and bounds on vortex spacing for lock-on to excitation frequency ( $\pm 1$  standard deviation) (dash-dot red); vs excitation frequency. Bounds on shear layer mode frequency (dashed purple) and jet preferred mode frequency (dashed green) also shown.

of the period of the flow field could then be built in a single, long experiment that produced around 1125 PIV frames. The signal-to-noise ratio was improved by using a moving window average 25 frames wide, giving 45 frames that illustrated a single period of the vortex shedding of the event at 300 Hz. This process was estimated to produce an uncertainty of 10% in the value of the shedding frequency.

Figure 11 clearly shows that the shear layer sheds vortices at the excitation frequency for frequencies at and above 1 kHz, as illustrated in Fig. 9. For 400–600 Hz, the vortices were produced at a harmonic of  $f_{ex}$  then merged to form vortices at  $f_{ex}$ . An example of this is shown in Fig. 12, which shows the 410 Hz case. The vortex spacing is initially smaller than the 1 kHz case (Fig. 9), but vortices are seen to merge

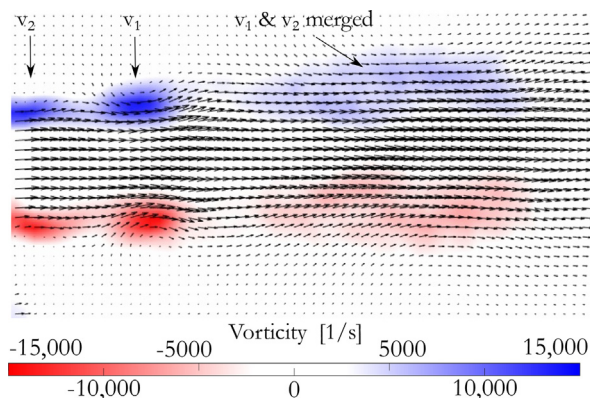


**FIG. 12.** Mean flow field with  $f_{ex} = 410$  Hz, showing vortex generation at a harmonic and merging event.

downstream. This can be judged from the approximate doubling of the spacing between the two distinct vortices close to the nozzle (labelled  $v_1$  and  $v_2$ , respectively) and between  $v_1$  and the larger, vortex downstream (labelled “ $v_1$  and  $v_2$  merged”).

No excitation frequencies between 700 and 950 Hz are shown in Fig. 11 because there were no coherent structures in the mean flow field, indicating that there was no lock-on in this range. At 300 Hz, lock-on occurs again with vortices produced at  $f_{ex}$ .

To test the limit of the vortex merging demodulation mechanism suggested in the literature,<sup>8,16</sup> the AM waveform in (5) was used to drive the loudspeaker. The carrier frequency was set to  $f_c = 2020$  Hz, which was chosen because it produced strong vortical structures. The modulating frequency was set to  $f_m = 0.5$  Hz, so that the response at  $f_m$  is fully resolved (no aliasing) and 100 PIV frames were sampled. Since the triggering rate was 10 Hz, this provided 20 snapshots through the modulating period. An ensemble of 5 PIV frames was averaged for each of the 20 points in the phase. The flow fields that show qualitatively the maximum and minimum vortex strength, which are  $180^\circ$  apart, are shown in Fig. 13, along with an intermediate phase.

In order to test the hypothesized Nyquist–Shannon sampling theorem analogy, an experiment was conducted with  $f_c = 2000$  and  $f_m = 1250$  Hz. The goal was to assess whether the response modulated onto the vortex train and subsequently demodulated in the vorticity signal is at  $f_m$  or the predicted alias frequency,  $f_c - f_m$ . The trigger frequency was set, so that 13.3 carrier periods were recorded over 2100 PIV frames. A 10-frame wide moving average window was applied before the power spectral density (PSD) of the vorticity timeseries was calculated at an ensemble of points in the shear layer and then averaged. This was repeated for several streamwise ranges of points to illustrate the evolution of the spectrum with downstream distance. The regions used for spatial averaging for each streamwise range are highlighted in Fig. 14, which shows the time-averaged vorticity field from this experiment. The PSDs are shown in Fig. 15. Vertical dash-dot lines are used to indicate the aliases of each of the relevant frequencies in the DC–5 Hz band for this trigger frequency. Note that the appearance of these frequencies at apparently much lower frequencies is related to the phase-averaging process rather than the aliasing effect of the shear layer that is the subject of this paper. It was possible to use regions on both sides of the jet and over a large streamwise distance because the averaging was conducted on the PSD, and the sign of the vorticity was not relevant.

As a second example, a lower carrier frequency was used to give a larger spacing between vortices, so that the shear layer vorticity signal could be studied in the time domain more easily. The frequencies  $f_c = 320$  and  $f_m = 240$  Hz were used, and the sampling frequency was set to give around four carrier periods over 1500 PIV frames. The vorticity in the shear layer was spatially averaged over two regions, which are shown in Fig. 16(a). A 10-frame-wide temporal moving average window was then applied to improve the signal-to-noise ratio. The resulting time series is shown in Fig. 17.

## V. DISCUSSION

The unexcited flow field in Figs. 6–8 represents baseline data. The presence or otherwise of coherent structures in the time-averaged vorticity field is a means of establishing whether or not vortices are shed at a multiple of the laser triggering frequency. For example, in the

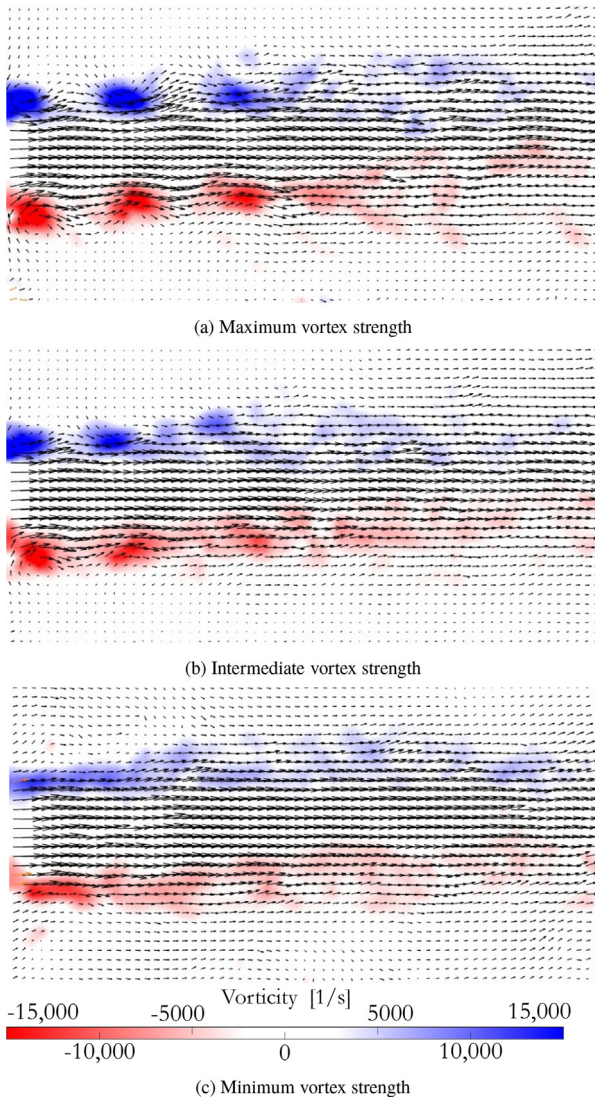


**FIG. 13.** Vorticity of ensemble-averaged flow fields with  $f_c = 2020$  Hz,  $f_m = 0.5$  Hz at several points in the phase corresponding to: (a) maximum vortex strength; (b) intermediate vortex strength; and (c) minimum vortex strength.

time-averaged, unexcited flow field in Fig. 7, the vorticity is smooth, and there are no coherent structures, whereas in the  $f_{ex} = 1$  kHz excitation case in Fig. 9, the vortices are clearly shed at a multiple of 10 Hz. The vortex shedding at a harmonic of  $f_{ex}$  for excitation frequencies in the range 400–600 Hz (Fig. 11) is an unexplained and uninvestigated result, which we report for the interested reader.

The response to AM excitation with  $f_c = 2020$  Hz,  $f_m = 0.5$  Hz in Fig. 13 shows “standing” vortices in each snapshot because the vortices are generated at  $f_c$ , which is a multiple of the trigger rate of 10 Hz. The three snapshots show that the strength of the vortex train varies at  $f_m$ . The maximum response case shows three vortex pairs clearly, while in the intermediate case, the third pair is less well-defined. The minimum case most closely resembles the unexcited, unaveraged

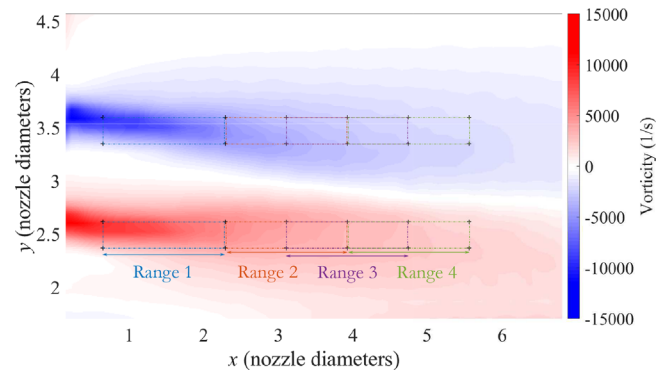


**FIG. 14.** Time-averaged vorticity field for  $f_c = 2000$  Hz,  $f_m = 1250$  Hz, with regions for spatial averaging used in Fig. 15.

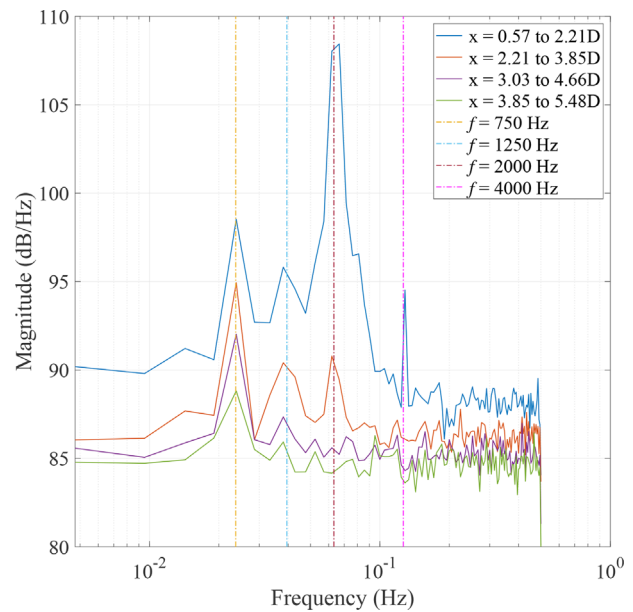


**FIG. 15.** Spatially averaged power spectral density of vorticity in shear layer over several regions in the shear layer,  $f_c = 2000$  Hz,  $f_m = 1250$  Hz. Frequencies corresponding to 750, 1250, and 2000 Hz indicated by dash-dot lines.

vorticity flow field snapshot in Fig. 8. The vortex merging demodulation mechanism suggested in the literature<sup>2,8</sup> clearly cannot happen in this case—4040 vortices would have to merge into a single vortex at  $f_m$ , but only around three vortex rings persist simultaneously in the flow field. These data support the perspective presented in Sec. III that the demodulation occurs because the vortex strength is modulated by the modulating component of the excitation signal. In this case, the demodulation happens when the vortices are created, rather than as a result of any vortex interaction.

The power spectral densities in Fig. 15 for  $f_c = 2000$  Hz,  $f_m = 1250$  Hz show a strong peak at the carrier frequency close to the nozzle orifice, which decays rapidly with downstream distance. The peak at 750 Hz is the second largest and persists further downstream than the carrier peak. This is consistent with the observations of

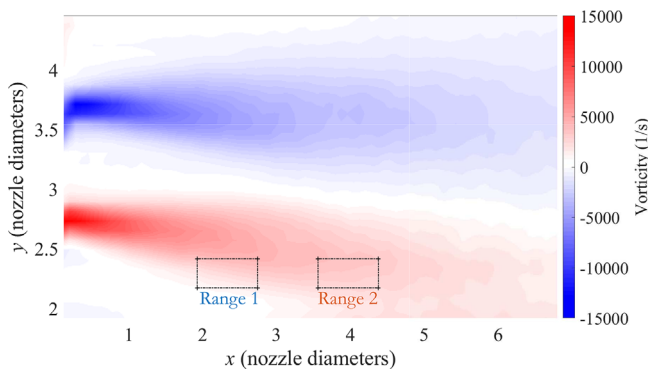


**FIG. 16.** Time-averaged vorticity field for  $f_c = 320$  Hz,  $f_m = 240$  Hz, with regions for spatial averaging used in Fig. 17.

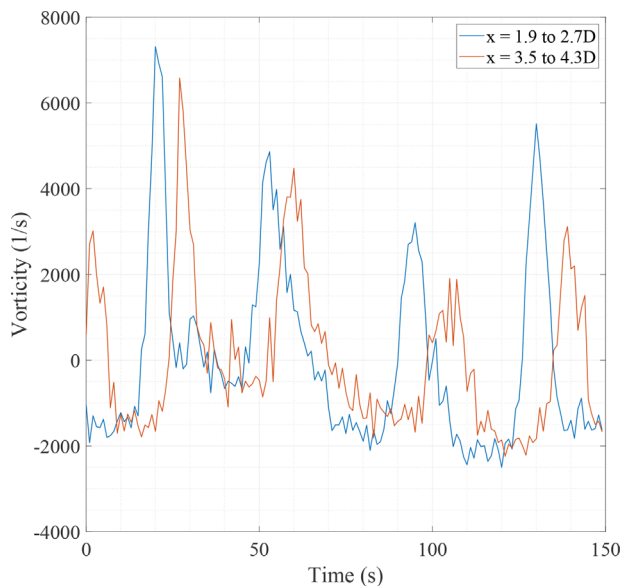


**FIG. 17.** Spatially averaged vorticity timeseries over two regions in one side of the shear layer,  $f_c = 320$  Hz,  $f_m = 240$  Hz.

Wiltse and Glezer<sup>2</sup> and Yehoshua and Seifert<sup>7</sup> the signal at  $f_c$  decays while the signal at the demodulated frequency survives for longer. It indicates that the demodulated frequency is at 750 Hz—the alias of the 1250 Hz modulating frequency. There is also a smaller peak at 1250 Hz, most likely a result of the fact that the 750 Hz waveform is not fully demodulated by the rectifying action of the vorticity signal—1250 Hz is the lower sideband of a 750 Hz envelope modulated onto a 2000 Hz carrier. The fact that the demodulated response is at the aliased frequency demonstrates that the Nyquist–Shannon sampling theorem applies.

The timeseries data for  $f_c = 320$  Hz,  $f_m = 240$  Hz in Fig. 17 show a strong vorticity signal corresponding to the vortex shedding frequency at  $f_c$ . The strength of each vortex is indicated by the size of the peak, which is modulated by an envelope. The periodicity of the envelope is the same for both streamwise ranges but is best observed in the

$x = 3.5\text{--}4.3 D$  (red) curve, which is shifted in time relative to the  $x = 1.9\text{--}2.7 D$  (blue) curve due to the finite convection speed of the vortices. The peak closest to  $t = 0$  is repeated at  $t \approx 140$  s, showing the periodicity of the envelope to be four carrier periods, i.e.,  $f_c - f_m = 80$  Hz, the aliased frequency, not  $f_m = 240$  Hz, the modulating frequency. This provides a time domain perspective of the aliased response.

The timeseries resemble the half-wave rectified vorticity model presented in Fig. 3(b), which is for the same case of  $f_m = 0.75f_c$ . The four distinct peaks in vorticity in the experimental data also match the vorticity model for case  $f_m = 0.25f_c$ , as predicted in Sec. III. The fact that the signals in Fig. 17 are half-wave rectified indicates that the envelope frequency at 80 Hz is present at baseband. Furthermore, this demonstrates that vortex merging is not required for demodulation in this case. Even if the vortices persisted for long enough and had sufficiently different speeds that merging could occur—which would undoubtedly increase the power at the demodulated frequency—it would be a result of the partial demodulation that has already taken place. This effect was clearly demonstrated by Yehoshua and Seifert<sup>7</sup> for the case of a synthetic jet in otherwise still air. Yehoshua and Seifert<sup>7</sup> attributed the demodulation mechanism to vortex merging (as well as the re-ingestion of sub-critical vortices), but the merging only occurred as a result of the modulation of strength of the vortex train, with its corresponding half-wave rectified (and therefore at least partially demodulated) vorticity signal. Vortex merging seems to be one of two demodulation mechanisms, and the data presented in this paper demonstrate that in some cases, it plays no role at all.

## VI. CONCLUSIONS

The signal processing perspective of jet shear layers proposed in this paper is centered on the idea that the vortices generated in the shear layer under acoustic excitation are like the samples of a digital system. The vortices “sample” the amplitude of the excitation tone, so that their strengths are determined by the modulating signal of an AM input. The vorticity signal resulting from the vortex train measured at a point in the shear layer resembles the half-wave rectified AM excitation signal. This is because the opposite sense vortices that could in theory be produced on the intake stroke of the loudspeaker membrane are offset by the natural, unexcited vorticity of the shear layer. A half-wave rectifier is a common implementation of an AM demodulator, which explains how the envelope of vortex strength is demodulated to baseband.

Viewing the system through this lens provides an alternative mechanism for the demodulation property discovered by Wiltse and Glezer<sup>2</sup> that does not rely on vortex merging. We have demonstrated that merging is not involved when either the distance between vortices is too large for them to interact (i.e., Fig. 17) or the modulating frequency is small relative to the carrier frequency, such that an impractically large number of vortices would be required to merge together into a single vortex (i.e., Fig. 13). Based on the experimental data presented here and in those of Yehoshua and Seifert,<sup>7</sup> vortex merging appears to be a consequence of partial demodulation that encourages further demodulation. Hence, merging is one of two demodulation mechanisms at play.

The corollary of the signal processing perspective of the shear layer is that the Nyquist–Shannon sampling theorem should apply, and using modulating frequencies that exceed half the carrier frequency should result in a vortex train that is modulated at the aliased



frequency, i.e.,  $f_c - f_m$ , rather than the modulating frequency,  $f_m$ . This was demonstrated both in the time and frequency domains in separate experiments, which underlines the insight provided by this point of view.

## ACKNOWLEDGMENTS

The authors gratefully acknowledge the support of this work by the EPSRC program grant (No. EP/P000878/1). We thank the reviewers and associate editor for their valued contributions to the paper.

## AUTHOR DECLARATIONS

### Conflict of Interest

The authors have no conflicts to disclose.

## Author Contributions

**Chris James Nicholls:** Conceptualization (lead); Data curation (equal); Formal analysis (lead); Investigation (lead); Methodology (equal); Writing – original draft (lead); Writing – review & editing (equal). **Kharthik Chakravarthy:** Data curation (equal); Formal analysis (supporting); Methodology (lead); Writing – review & editing (supporting). **Brian Ming Tak Tang:** Formal analysis (supporting); Writing – review & editing (equal). **Benjamin Williams:** Funding acquisition (equal); Resources (lead). **Marko Bacic:** Formal analysis (supporting); Funding acquisition (lead); Writing – review & editing (supporting).

## DATA AVAILABILITY

The data that support the findings of this study are available from the corresponding author upon reasonable request.

## REFERENCES

- <sup>1</sup>S. C. Crow and F. H. Champagne, “Orderly structure in jet turbulence,” *J. Fluid Mech.* **48**, 547–591 (1971).
- <sup>2</sup>J. M. Wiltse and A. Glezer, “Manipulation of free shear flows using piezoelectric actuators,” *J. Fluid Mech.* **249**, 261–285 (1993).
- <sup>3</sup>B. L. Smith and A. Glezer, “Jet vectoring using synthetic jets,” *J. Fluid Mech.* **458**, 1 (2002).
- <sup>4</sup>D. Rapoport, I. Fono, K. Cohen, and A. Seifert, “Closed-loop vectoring control of a turbulent jet using periodic excitation,” *J. Propul. Power* **19**, 646–654 (2003).
- <sup>5</sup>C. J. Nicholls and M. Bacic, “Closed-loop control of a piezo-fluidic amplifier,” *AIAA J.* **58**, 2414–2427 (2020).
- <sup>6</sup>S. A. Jacobson and W. C. Reynolds, “Active control of streamwise vortices and streaks in boundary layers,” *J. Fluid Mech.* **360**, 179–211 (1998).
- <sup>7</sup>T. Yehoshua and A. Seifert, “On the evolution of amplitude modulated excitation in still air,” *Int. J. Flow Control* **3**, 171–191 (2011).
- <sup>8</sup>B. Vukasinovic, D. Lucas, and A. Glezer, “Direct manipulation of small-scale motions in a plane shear layer,” AIAA Paper No. 2004-2617, 2004.
- <sup>9</sup>M. Mair, “On dynamics of fluidic jet switching and shear layer instabilities,” Ph.D. thesis (University of Oxford, 2019).
- <sup>10</sup>C.-W. Kuo, J. Cluts, and M. Samimy, “Effects of excitation around jet preferred mode Strouhal number in high-speed jets,” *Exp. Fluids* **58**, 35 (2017).
- <sup>11</sup>M. Mair, M. Bacic, K. Chakravarthy, and B. Williams, “Jet preferred mode vs shear layer mode,” *Phys. Fluids* **32**, 064106 (2020).
- <sup>12</sup>K. B. M. Q. Zaman and A. K. M. F. Hussain, “Vortex pairing in a circular jet under controlled excitation. Part 1. General jet response,” *J. Fluid Mech.* **101**, 449–491 (1980).
- <sup>13</sup>M. Samimy, N. Webb, and M. Crawley, “Excitation of free shear-layer instabilities for high-speed flow control,” *AIAA J.* **56**, 1770–1791 (2018).
- <sup>14</sup>H. Nyquist, “Certain topics in telegraph transmission theory,” *Trans. Am. Inst. Electr. Eng.* **47**, 617–644 (1928).
- <sup>15</sup>C. E. Shannon, “Communication in the presence of noise,” *Proc. IRE* **37**, 10–21 (1949).
- <sup>16</sup>A. Glezer and M. Amitay, “Synthetic jets,” *Annu. Rev. Fluid Mech.* **34**, 503–529 (2002).